The Interdecadal Variations and Causes of the Relationship Between Autumn Precipitation Anomalies in Eastern China and SSTA Over the Southeastern Tropical Indian Ocean

Liwei Huo
Nanjing University of Information Science and Technology
Zhaoyong Guan (guanzy@nuist.edu.cn)
Nanjing University of Information Science and Technology
Dachao Jin
Nanjing University of Information Science and Technology
Xi Liu
Jiangsu Institute of Meteorology Sciences
Xudong Wang
Fudan University
Yang Xia
Liupanshui Meteorological Bureau

Research Article

Keywords: Interdecadal Variations, Relationship, Precipitation Anomalies, Eastern China, Indian Ocean, population, economy, correlations

Posted Date: December 13th, 2021

DOI: https://doi.org/10.21203/rs.3.rs-1150525/v1

Abstract

Eastern China has a large population with rapid development of the economy, where is the important crop producing region. In this region, the spatial and temporal distribution of autumn rainfall in Eastern China is uneven, which has important societal impact. Using the NCEP–NCAR reanalysis and other observational datasets, it is found that the spatial distribution of the first EOF mode of autumn rainfall anomalies in eastern China is consistent across the region, with significant interannual variabilities. Pronounced interdecadal variations are presented in the relationship between autumn rainfall anomalies in eastern China and sea-surface temperature anomalies (SSTA) over the southeastern tropical Indian Ocean (SETIO). The interdecadal changes have been analyzed by considering two epochs: one during 1979-2004 and the other during 2005-2019. It shows weak and insignificant correlations between the autumn rainfall anomalies in eastern China and SSTA over SETIO during the first epoch. On the other hand, they are remarkable and positively correlated with each other during the second epoch. The inter-decadal changes of the above relationship are related to the warming of SST over SETIO during the second epoch. It causes stronger low-level convergence and ascending motion over SETIO, with the co-occurrence of enhanced western Pacific subtropical high and anomalous abundant moisture over eastern China carried by a low-level southerly anomaly originating from the South China Sea. Simultaneously, the local Hadley circulation over eastern China becomes weak, corresponding to the anomalous ascending motion. The collaboration of anomalous water vapour transport and ascending motion strengthens the connection between the SETIO SSTA and the autumn precipitation anomalies in eastern China, and vice versa. In the boreal autumn of 2019, entire eastern China suffered extreme drought. It suggests that this drought event in eastern China is strongly affected by the negative SSTA over SETIO, which is consistent with the statistical results.

1. Introduction

Eastern China is adjacent to the Northwest Pacific Ocean, and locates in the East Asian monsoon region, with a vast territory and complex climatic fluctuations (Tao & Chen 1987; Ding 2004). As is well known, eastern China is the most economically developed and densely populated area of China, with a geographical concentration of large cities. Within this large area, the rainy season is concentrated in summer (Ding 2004; Jin et al. 2015). The temporal and spatial variation of summer precipitation in eastern China and its causes have received great attention in recent years (e.g. Tao & Chen 1987; Huang & Wu 1989; Ding 2004; Ding et al. 2008; Huang et al. 2012; Jin et al. 2015). Likewise, there are significant interannual and interdecadal variability in the autumn precipitation anomalies in eastern China (Ying et al. 2015; Yuan & Wang 2019), which could cause severe climate impacts. The extreme drought event in eastern China during the autumn in 2019 produced damaging impacts on local residential life as well as societal and economic development.

The precipitation anomalies in eastern China is regulated by many factors, such as El Niño–Southern Oscillation (ENSO) and sea surface temperature anomalies (SSTA) in the Indian Ocean. ENSO is the leading mode of climate variability in tropical regions. Its warm phase, namely the El Nino event, can

affect the western Pacific subtropical high through local air-sea interactions (Wang et al. 2000, 2013), which in turn affects precipitation anomalies in eastern China (e.g., Wu And Wang 2002; Jin et al., 2016). The Indian Ocean basin-scale warming (Chambers et al., 1999; Xie et al., 2009) can also affect the atmospheric circulation anomalies in East Asia through the “capacitor” effect (Xie et al. 2009) or the “two-stage thermal adaptation” mechanism (Wu et al., 2000), and further affects the climate anomalies in East Asia (Wu et al., 2010; He et al. 2015; Xie et al. 2016).

Southeastern Tropical Indian Ocean (SETIO) is the eastern pole of the Indian Ocean Dipole (IOD; Saji et al., 1999), where is close to the tropical western Pacific Ocean. The SSTA over SETIO appears to affect the climate anomaly of the adjacent area (eg: Wu et al., 2010; Chen et al., 2016; Huo and Jin, 2016). The SETIO SSTA could influence the anomalous precipitation over southern China by adjusting the anomalous water vapour transport and the local Hadley circulation (Huo and Jin, 2016). The above relationship has significant interdecadal changes (Chen et al., 2016; Wu et al., 2010).

Previous studies documented the remarkable interdecadal variations of the anomalous autumn precipitation over eastern China. Before the 1990s, the autumn precipitation anomalies in eastern China presented a quasi-meridional dipole mode, which appeared to be not obvious after that. Yuan and Wang (2019) suggests that this change is closely associated with the interdecadal variations of ENSO. The above conclusions motivated this study. If the ENSO signal is filtered out, is there any possible connection can be found between the autumn precipitation anomalies in eastern China and SSTA in SETIO? If the answer is true, what are the possible mechanisms behind this relationship? It is also unclear whether the link between the two is stable. In the present paper, we investigated these possibilities by looking at the autumn rainfall anomaly over eastern China and its association with the SETIO SSTA on the interdecadal timescale. We further analyzed the possible mechanisms of SETIO SSTA influencing the extreme drought event in eastern China during the autumn of 2019.

This paper is organized as follows. Section 2 introduces the data and method that are used. Section 3 explores the temporal and spatial variations of autumn precipitation in eastern China. In Section 4, the interdecadal variations of the relationship between autumn rainfall anomaly over eastern China and the SETIO SSTA are investigated. The mechanism behind the above relationship is discussed in Section 5. In Section 6, we discuss the influence of the negative SETIO SSTA on the extreme drought event in eastern China during the autumn of 2019. The conclusions are given in the last section.

2. Data And Methodology

We obtained rainfall observations of 2479 stations in China at daily resolution from the National Meteorological Information Center of China Meteorological Administration. From this we chose 604 stations located in eastern China for our analysis (Figure 1a), after excluding those with data missing. The Extended Reconstructed Sea Surface Temperature (ERSST v3b, Smith et al. 2008) data from the National Oceanic and Atmospheric Administration (NOAA) with a horizontal resolution of 2°×2°, and the NCEP–NCAR reanalysis (Kalnay et al. 1996) with the horizontal resolution of 2.5°×2.5° are also used in

this study. All these datasets cover the period of 1979–2019. Boreal autumn months in the present work are September–November (SON). Eastern China (110°E -124°E, 24°N-35°N) is the mainland China area as shown in Figure 1a.

To focus on the interannual variations of SSTA over the tropical Indian Ocean, long-term trends and periodicities of 9 years and longer are removed but in Figure 1a. The Nino3.4 index used in this paper is the regional average SSTA in the geographic region [170°W–120°W, 5°S–5°N]. The ENSO signal can affect the Indian Ocean SSTA (e.g., Saji & Yamagata, 2003; Xie et al., 2009; Doi et al., 2020), and rainfall anomaly over eastern China (Jin et al., 2016; Yuan & Wang, 2019). To explore the relationship between rainfall anomaly over eastern China and Indian Ocean SSTA, ENSO signal indicated by the Nino3.4 index is excluded by using the linear regression method as follows:

$$Y = \alpha \times I_{\mathrm{Nino3.4}} + Y_r \qquad (1)$$

In Eq. (1), Y stands for the time series of variables of interest. $I_{\mathrm{Nino3.4}}$ stands for the normalized time series of the autumn ENSO index. Y_r stands for the residual value of the variable Y after the ENSO signal is removed. Coefficient α is the covariance of Y and $I_{\mathrm{Nino3.4}}$.

3. Temporal And Spatial Variations Of Autumn Rainfall Over Eastern China

Climatologically, the distribution of autumn precipitation over eastern China is very uneven in spatial. It decreases in amplitude from the south to the north (Figure 1a). Coastal areas of southern and southeastern China receive the most abundant rainfall with values exceeding 300 mm. The maximum value is larger than 360 mm. Markedly low rainfall is found to the north of 33°N, with minimum values smaller than 150 mm.

Based on the empirical orthogonal function (EOF) analysis, the first EOF mode (EOF1) shows spatially consistent autumn precipitation anomalies (Figure 1b), consistent with the previous study (Yuan and Wang, 2019). EOF1 explains about 29.8% of the total variances, EOF1 can be effectively separated from the second EOF mode (North, 1982). Higher loadings are located in central and southern South China, whereas lower loadings are distributed to the north of the Yangtze River. The time series of EOF1 (Figure 1c) presents significant interdecadal variability. The correlation coefficient between the time sequence of EOF1 and mean autumn precipitation anomalies over eastern China is as high as 0.93. It further demonstrates that the main mode of the autumn precipitation anomalies over eastern China is consistent across the whole region.

Noted that normalized time series of EOF1 and mean autumn precipitation anomalies over eastern China in 2019 are both smaller than their minus two standard deviations (Figure 1c), which are their minimum values during the recent 40 years. Figure 1d shows that the mean autumn precipitation anomaly in 2019

and its percentage are negative over eastern China. The minimum rainfall areas are located in the central and adjacent areas of Jiangxi Province, southern China, and the coastal areas of Jiangsu and Zhejiang Province. The minimum precipitation value is less than -250 mm, with a minimum percentage of less than -90%.

4. Relationship Between The Autumn Precipitation Anomalies Over Eastern China And Southeastern Tropical Indian Ocean Ssta

As concluded by Saji et al. (1999), the positive phase of IOD is described as the negative SSTA over SETIO and positive SSTA over the western tropical Indian Ocean. The IOD presents an extreme positive phase during the autumn in 2019 (Doi et al., 2020), corresponding to the negative anomalous autumn precipitation over eastern China as discussed above. It inspires us to explore the relationship between the extreme autumn drought over eastern China and the SSTA over the tropical Indian Ocean in 2019.

To answer this question, we calculate the correlation coefficients of the precipitation anomaly averaged over eastern China (P_{EC}) and SSTA averaged over SETIO (I_{SETIO}), the western pole of IOD and IOD index, which is 0.39, 0.06 and -0.22, respectively. Since ENSO is closely associated with IOD (Saji & Yamagata, 2003; Doi et al., 2020) and also the precipitation anomaly over eastern China (Jin et al., 2016; Yuan & Wang, 2019), the above correlation coefficients are calculated by further excluding the ENSO signal. After filtering the ENSO signal, the correlation coefficients between P_{EC} and the western pole of IOD, P_{EC} and IOD index are still not strong with the value of 0.21 and -0.15, respectively. The correlation coefficient between P_{EC} and I_{SETIO} is 0.36, indicating their intrinsic relations. Time series of I_{SETIO} (Figure 2a) suggests that I_{SETIO} is dramatically anomalous negative in 2019, with the value of about minus two standard deviations.

To further clarify the relationship between P_{EC} and I_{SETIO}, we calculate the 11-year sliding correlation coefficient between the two, showing a significant interdecadal variation between P_{EC} and I_{SETIO} (Figure 2b). Before 2005, the correlation between P_{EC} and I_{SETIO} gradually evolves from a weak positive correlation to a weak negative correlation. After that, P_{EC} is closely related to I_{SETIO} with the correlation coefficient during 2010-2014, exceeding the 95% significance level. Thus, we consider 2005-2019 as the closely related period, while 1979-2004 as the unrelated period. The correlation coefficients between P_{EC} and I_{SETIO} during 1979-2004 and 2005-2019 are 0.04 and 0.74, respectively. It indicates that precipitation anomaly over eastern China and SETIO SSTA has an enhanced interdecadal relationship. During 1979-2004, P_{EC} is positively related to SSTA over the central Tropical Indian Ocean with values smaller than 0.4 in most areas (Figure 2c). But P_{EC} is significantly associated with the SETIO SSTA during 2005-2019 (Figure 2d), with values larger than 0.4 in most areas.

As shown in Figure 3a, SETIO SSTA is weakly correlated with the P_{EC} over limited areas of coastal southeastern China and to the north of the Yangtze River during 1979-2004. During 2005-2019, evident positive correlations between P_{EC} and I_{SETIO} are broadly distributed over most areas of eastern China

(Figure 3b), especially over the middle and lower reaches of the Yangtze River and South China. The scatter plot of I_{SETIO} and P_{EC} during 1979-2019 (Figure 4a) suggests that even positive correlations between I_{SETIO} and P_{EC} are evident, most of I_{SETIO} and P_{EC} pairs are away from the linear fitted line indicating their weak linear relation. As further shown in Figure 4b and 4c, P_{EC} is not linear related to I_{SETIO} during 1979-2004, but is highly linear related to I_{SETIO} during 2005-2019 with a linear fitted index of 0.83.

5. Possible Mechanisms

To discover the possible mechanisms resulting in the interdecadal variability of the relationship between P_{EC} anomaly and SETIO SSTA, especially the closer relationship after 2005, anomalous atmospheric circulations associated with the SETIO SSTA are analyzed in the following.

5.1 Anomalous stream function and rotational wind

During 1979-2004, the 850-hPa stream function and rotational wind regressed from I_{SETIO} (Figure 5a) shows that there exists a pair of anomalous cyclonic circulations and anomalous westerly flows over the equatorial Indian Ocean stretching from the tropical to subtropical regions, due to the Mastuno-Gill response to the SETIO SSTA (Mastuno, 1966; Gill, 1980). The anomalous cyclonic circulation in the northern hemisphere is more zonal-elongated (40°E-140°E). Eastern China is under the influence of this anomalous cyclonic circulation. Vice versa.

As shown in Figure 5b, the anomalous cyclonic circulation is located from the Bay of Bengal to the Indochina Peninsula and adjacent areas during 2005-2019, corresponding to the anomalous cyclonic circulation in the southern hemisphere. Due to the Kelvin wave response to SST warming over SETIO (Mastuno, 1966; Gill, 1980), the easterly flow anomalies over the western Pacific Ocean could enhance the western Pacific subtropical high and contribute to the anomalous southerly flows over eastern China.

Comparing the anomalous circulation associated with I_{SETIO} during the two periods (1979-2004 vs 2005-2019), there both exist the response of Rossby wave associated with the positive SETIO SSTA. The anomalous cyclonic circulation is more zonal-elongated during 1979-2004, whereas is confined in relatively small areas over South China and Indochina Peninsula during 2005-2019, associated with the intensification and westward extension of the western Pacific subtropical high.

5.2 Anomalous water vapour transport

From 1979 to 2004, the integrated water vapour flux and its divergence regressed from I_{SETIO} (Figure 6a) shows that there is anomalous water vapour transport from the west to the east in the tropical Indian Ocean, resulting in the anomalous water vapour convergence over SETIO. Part of the water vapour is transported from the tropical Indian Ocean, passing through Java Islands, the South China Sea and the Kuroshio area, then transported westward to eastern China, and finally to South Asia along the southern

foot of the Tibetan Plateau. Anomalous water vapour divergence is distributed in some areas of eastern China, which is consistent with the anomalous circulation in the lower troposphere (Figure 5a).

As for the period of 2005-2019, a pair of cyclonic circulations is located along the equatorial Indian Ocean, corresponding to the eastward water vapour transport anomaly. Anomalous water vapour flux over the tropical western Pacific Ocean is transported to eastern China along the edge of the western Pacific subtropical high. The water vapour is anomalous convergence over eastern China, favoring the above-normal autumn precipitation over eastern China. Vice versa.

5.3 Vertical motion analysis

During 1979-2004, the positive SETIO SSTA corresponds to the anomalous lower-level convergence (Figure 7a), upper-level divergence (Figure 7b) and associated ascending motion (Figure 7c) over the Maritime Continent. To the opposite, the tropical western Indian Ocean and the African continent are regulated by anomalous lower-level divergence (Figure 7a), upper-level convergence (Figure 7b) and associated descending motion (Figure 7c). Whereas eastern China has no anomalous vertical motions (Figure 7c).

Similar to the period of 1979-2004, SETIO is featured with the anomalous lower-level convergence (Figure 7d), upper-level divergence (Figure 7e) and associated ascending motion (Figure 7f) during 2005-2019, corresponding to the positive SETIO SSTA. But the northwestern Pacific Ocean is characterized by anomalous divergence at the lower troposphere and the strengthened western Pacific subtropical high during 2005-2019 (Figure 7d). Noted that the anomalous convergence, divergence and ascending motions over SETIO during 2005-2019 are all stronger than that during 1979-2004. Eastern China is controlled by the anomalous convergence at the lower troposphere, divergence at the upper troposphere, and ascending motions, which is favorable for the above-normal autumn precipitation over eastern China.

The climatological mean equatorial zonal-vertical circulation over the tropical eastern Indian Ocean and Pacific Ocean (Figure 8a) indicates that areas from the tropical eastern Indian Ocean to the central Pacific Ocean are controlled by anomalous ascending motion, whereas the tropical western Pacific ocean is dominated by anomalous descending motion, that is known as the Walker Circulation. The difference of the unfiltered SSTA averaged over SETIO between the two periods, i.e. 2005-2019 and 1979-2004, is 0.2°C. Differences of the regressed equatorial zonal–vertical circulation with respect to the I_{SETIO} for 2005-2019 and 1979-2004 (Figure 8b) present the strengthened anomalous ascending motion over tropical eastern Indian Ocean and anomalous descending motion over tropical western Pacific Ocean. This would produce the anomalous low-level divergence over the western Pacific Ocean, and strengthen the western Pacific subtropical high (Figures 5 and 7a-b). The integrated water vapour transported from the western Pacific Ocean to eastern China can subsequently be strengthened, providing abundant water vapour for the enhancement of the connection between SETIO SSTA and the anomalous autumn precipitation in eastern China.

As shown in Figure 8c, the ascending branch of eastern China is distributed between the equator to 20°N, with two descending branches locating at its north and south. The difference of regressed zonal-vertical circulation between the two periods demonstrates that the warming SETIO SSTA is corresponding to the enhancement of anomalous ascending motion over SETIO, weakening of the ascending motion at 5°N-20°N and subsequently strengthened ascending motion over eastern China (25°N-30°N). It shows a circulation pattern of strengthened local Hadley circulation over eastern China, providing favorable vertical motion conditions for the enhanced connection between SETIO SSTA and the anomalous autumn precipitation in eastern China.

6. Analysis Of The Extreme Drought In 2019

The spatial distribution of SSTA over the tropical Indian Ocean in 2019 presents the negative SSTA over SETIO with a minimum of smaller than -1°C (Figure 9a). A pair of anti-cyclonic circulations on 850 hPa (Figure 9b) is induced across the equator to the west of SETIO, and is corresponding to the anomalous westerlies along the equator (Mastuno, 1966; Gill, 1980). The anomalous cyclonic circulation over the northwest Pacific Ocean is indicative of a weakening northwest Pacific subtropical high (Figure 9b). SETIO is characterized by the anomalous divergence in the lower troposphere (Figure 9c) and anomalous convergence in the upper troposphere (Figure 9d). On the contrary, the northwest Pacific ocean is controlled by the anomalous convergence in the lower troposphere (Figure 9c) and anomalous divergence in the upper troposphere (Figure 9d). The enhanced locally Hadley circulation over eastern China consists of the anomalous subsidence over SETIO and eastern China, and the anomalous ascending motion over the South China Sea (Figure 9e). It is also noted that a water vapour transport anomaly toward the equator over eastern China (Figure 9f) and reducing the water vapour transport from the western Pacific Ocean to eastern China. The combination of the above conditions caused the persistent autumn drought over eastern China in 2019 (Figure 1d).

7. Discussion And Conclusions

This study investigates the interdecadal variations of the relationship between autumn precipitation anomaly over eastern China and SSTA over SETIO during the past 40 years (1979-2019). Possible mechanisms of the negative anomaly of SETIO SSTA on the autumn drought in eastern China in 2019 are also discussed. The conclusions are as follows:

(1) Autumn precipitation over eastern China is unevenly distributed in spatial and temporal perspective, with significant interannual variability. The first EOF mode of autumn precipitation anomaly over eastern China is consistent across the whole region. The autumn precipitation anomaly over eastern China in 2019 is smaller than minus two standard deviations.

(2) The relationship between autumn precipitation anomalies in eastern China and SETIO SSTA has significant interdecadal changes. Before 2005, there is no significant relationship between the two, after which there is a significant positive correlation.

(3) From 1979-2004, the anomalous atmospheric circulation associated with SSTA over SETIO is indicative of a zonal-elongated cyclonic circulation anomaly from Arabian Peninsula to eastern China, the anomalous eastward extension of the western Pacific subtropical high, the anomalous water vapour divergence over eastern China and adjacent areas, and the absence of anomalous ascending motions. During 2005-2019, SSTA over SETIO is responsible for the westward extension of the western Pacific subtropical high, which could further enhance the water vapour transport toward eastern China and induce anomalous ascending motions over eastern China. The relationship between SSTA over SETIO and anomalous autumn precipitation over eastern China is subsequently strengthened, which is closely related to the warmer SST over SETIO during 2005-2019.

(4) In the autumn of 2019, the negative SSTA over SETIO weakened the western Pacific subtropical high, which is not conducive to the water vapour transport to eastern China and weakened the ascending motion over there. The collaboration of the above conditions contributed to the extreme autumn drought over eastern China in 2019.

It should be noted that the first EOF mode of the autumn precipitation anomaly in eastern China is consistent across the region, and the second EOF mode presents a north-south dipole pattern. Such dipole mode disappeared in the mid-to-late 1980s (Yuan and Wang, 2019). It requires further research to explore whether the disappearance of the dipole mode is related to the warming SST over SETIO. It is still unknown why the autumn precipitation is related to the SSTA over SETIO where is the eastern pole of IOD (Saji et al., 1999), but shows little correlations with the SSTA over the western pole of IOD. The influences of the SSTA over the western Pacific Ocean on the autumn precipitation also need further research in the future, considering the close relationship between the SSTA over the western Pacific Ocean and eastern Asian climate anomalies (Ham et al., 2013; Chen et al., 2015; Huo et al., 2015; Chen et al., 2018; Jin and Huo, 2018; Zuo et al., 2019).

Declarations

Acknowledgements

This research is supported by the National Key R&D Program of China (2019YFC1510201), the National Natural Science Foundation of China (Grants 42005016, 41905061).

References

1. Chambers D. P., Tapley B. D., Stewart R. H., 1999: Anomalous warming in the Indian Ocean coincident with El Niño. J Geophys Res 104: 3035–3047.
2. Chen J, Wen Z, Wu R, Wang X, He C, Chen Z., 2016: An interdecadal change in the intensity of interannual variability in summer rainfall over southern China around early 1990s. Climate Dynamics, doi: 10.1007/s00382-016-3069-8.

3. Chen, J., X. Wang, W. Zhou, C. Wang, Q. Xie, G. Li, and S. Chen, 2018: Unusual Rainfall in Southern China in Decaying August during Extreme El Niño 2015/16: Role of the Western Indian Ocean and North Tropical Atlantic SST. J. Climate, 31, 7019–7034, https://doi.org/10.1175/JCLI-D-17-0827.1.
4. Chen W, Lee J-Y, Lu R, Dong B, Ha K-J., 2015: Intensified impact of tropical Atlantic SST on the western North Pacific summer climate under a weakened Atlantic thermohaline circulation. Clim Dyn 45:2033–2046. https://doi.org/10.1007/s00382-014-2454-4.
5. Ding, Y., 2004: Seasonal march of the East Asian summer monsoon. East Asian Monsoon, C. P. Chang, Ed., World Scientific Publishing, 3–53.
6. Ding, Y., Z. Wang, and Y. Sun, 2008: Inter-decadal variation of the summer precipitation in east China and its association with decreasing Asian summer monsoon. Part I: Observed evi- dences. Int. J. Climatol., 28, 1139–1161, doi:10.1002/joc.1615.
7. Doi, T., Behera, S. K., and Yamagata, T., 2020: Predictability of the super IOD event in 2019 and its link with El Niño Modoki. Geophysical Research Letters, 47, e2019GL086713.
8. Gill, A.E., 1980: Some simple solutions for heat-induced tropical circulation. Quarterly Journal of the Royal Meteorological Society, 106, 447–462. https:// doi.org/10.1002/qj.49710644905.
9. He, C., Zhou, T., and Wu, B., 2015: The key oceanic regions responsible for the interannual variability of the western North Pacific subtropical high and associated mechanisms. J Meteorol Res 29, 562–575. https://doi.org/10.1007/s13351-015-5037-3.
10. Ihara, C., Y. Kushnir, and M.A. Cane, 2008: Warming Trend of the Indian Ocean SST and Indian Ocean Dipole from 1880 to 2004. J. Climate, 21, 2035–2046, https://doi.org/10.1175/2007JCLI1945.1.
11. Ham, Y.-G., J.-S. Kug, J.-Y. Park, and F.-F. Jin, 2013: Sea surface temperature in the north tropical Atlantic as a trigger for El Niño/Southern Oscillation events. Nat. Geosci., 6, 112–116, doi:10.1038/ngeo1686.
12. Huang R., and Y. Wu, 1989: The influence of ENSO on the summer climate change in China and its mechanism. Adv. Atmos. Sci., 6, 21–32, doi:10.1007/BF02656915.
13. Huang R., J. Chen, L. Wang, and Z. Lin, 2012: Characteristics, pro- cesses, and causes of the spatio-temporal variabilities of the East Asian monsoon system. Adv. Atmos. Sci., 29, 910–942, doi:10.1007/s00376-012-2015-x.
14. Huo Liwei, Guo Pinwen, Saji Hameed, and Jin Dachao, 2015: The role of tropical Atlantic SST anomalies in modulating western North Pacific tropical cyclone genesis. Geophys. Res. Lett.,42, 2378–2384. doi: 10.1002/2015GL063184.
15. Huo L., and Jin D., 2016: The interannual relationship between anomalous precipitation over southern China and the south eastern tropical Indian Ocean sea surface temperature anomalies during boreal summer. Atmosph. Sci. Lett.,17: 610–615. doi: 10.1002/asl.710.
16. Jin, D., Guan Z., J. Cai, and W. Tang, 2015: Interannual variations of regional summer precipitation in mainland China and their possible relationships with different teleconnections in the past five decades. J. Meteor. Soc. Japan, 93, 265–283, doi:10.2151/jmsj.2015-015.

17. Jin, D., S. Hameed, and L. Huo, 2016: Recent changes in ENSO teleconnection over the western Pacific impacts the eastern China precipitation dipole. J. Climate, 29, 7587–7598, doi:10.1175/JCLI-D-16-0235.1.
18. Jin Dachao, Huo Liwei. 2018: Influence of tropical Atlantic sea surface temperature anomalies on the East Asian summer monsoon. Q J R Meteorol Soc. 1490–1500. https://doi.org/10.1002/qj.3296.
19. Kalnay E., Kanamitsu M., Kistler R., et al., The NCEP/NCAR 40-Year Reanalysis Project. Bull Amer Meteor Soc, 1996, 77(3) : 437-471
20. Krishnamurthy, L., and Krishnamurthy, V., 2016 Decadal and interannual variability of the Indian Ocean SST. Clim Dyn 46, 57–70. https://doi.org/10.1007/s00382-015-2568-3.
21. Matsuno, T., 1966: Quasi-geostrophic motions in the equatorial area. Journal of the Meteorological Society of Japan, 44, 25–43. https://doi.org/10.2151/ jmsj1965.44.1_25.
22. North, G.R., T.L. Bell, R.F. Cahalan, and F.J. Moeng, 1982: Sampling Errors in the Estimation of Empirical Orthogonal Functions. Mon. Wea. Rev., 110, 699–706, https://doi.org/10.1175/1520-0493(1982)110<0699:SEITEO>2.0.CO;2
23. Saji, N. H., Goswami, B. N., Vinayachandran, P. N., & Yamagata, T., 1999: A dipole mode in the tropical Indian Ocean. Nature, 401(6751), 360–363. https://doi.org/10.1038/43854
24. Saji, N. H., & Yamagata, T., 2003: Possible impacts of Indian Ocean Dipole mode events on global climate. Climate Research, 25(2), 151–169. https://doi.org/10.3354/cr025151.
25. Smith, T.M., R.W. Reynolds, T.C. Peterson, and J. Lawrimore, 2008: Improvements NOAAs Historical Merged Land–Ocean Temp Analysis (1880–2006). Journal of Climate, 21, 2283–2296.
26. Tao, S., and L. Chen, 1987: A review of recent research on the East Asian summer monsoon in China. Monsoon Meteorology, C. P. Chang and T. N. Krishnamurti, Eds., Oxford University Press, 60–92.
27. Wang B, R. Wu, and X. Fu. 2000: Pacific–east Asian teleconnection: How does ENSO affect east Asian climate? Journal of Climate, 13, 1517–1536.
28. Wang B, Xiang B, Lee J Y. 2013: Subtropical high predictability establishes a promising way for monsoon and tropical storm predictions. Proceedings of the National Academy of Sciences, 110(8): 2718-2722.
29. Wu, B., T. Li, and T. Zhou, 2010: Relative Contributions of the Indian Ocean and Local SST Anomalies to the Maintenance of the Western North Pacific Anomalous Anticyclone during the El Niño Decaying Summer. J. Climate, 23, 2974–2986, https://doi.org/10.1175/2010JCLI3300.1.
30. Wu G., Liu Y., 2000: Thermal Adaptation, Overshooting, Dispersion, and Subtropical Anticyclone Part I: Thermal Adaptation and Overshooting.Chinese Journal of Atmospheric Sciences (in Chinese), 24(4):433-446.
31. Wu, R. and B. Wang, 2002: A Contrast of the East Asian Summer Monsoon–ENSO Relationship between 1962–77 and 1978–93. J. Climate, 15, 3266–3279, https://doi.org/10.1175/1520-0442(2002)015<3266:ACOTEA>2.0.CO;2.

32. Wu R, Wen Z, Yang S, Li Y. 2010. An interdecadal change in south- ern China summer rainfall around 1992/93. Journal of Climate 23: 2389–2403, doi: 10.1175/2009JCLI3336.1.
33. Xie, S., K. Hu, J. Hafner, H. Tokinaga, Y. Du, G. Huang, and T. Sampe, 2009: Indian Ocean Capacitor Effect on Indo–Western Pacific Climate during the Summer following El Niño. J. Climate, 22, 730–747, https://doi.org/10.1175/2008JCLI2544.1.
34. Xie, S. P., Y. Kosaka, Y. Du, et al., 2016: Indo-western Pacific Ocean capacitor and coherent climate anomalies in post-ENSO summer: A review. Adv. Atmos. Sci., 33, doi:10.1007/s00376-015-5192-6.
35. Ying, K., Zhao, T., Quan, X. et al., 2015: Interannual variability of autumn to spring seasonal precipitation in eastern China. Clim Dyn 45, 253–271. https://doi.org/10.1007/s00382-014-2411-2.
36. Yuan, C, Wang, D., 2019: Inter-decadal variations in El Niño–Southern Oscillation impacts on the autumn precipitation in the eastern China. Int J Climatol. 2019; 39: 5316-5326. https://doi.org/10.1002/joc.6156.
37. Zuo, J., Li, W., Sun, C. et al., 2019: Remote forcing of the northern tropical Atlantic SST anomalies on the western North Pacific anomalous anticyclone. Clim Dyn 52, 2837–2853. https://doi.org/10.1007/s00382-018-4298-9.

Figures

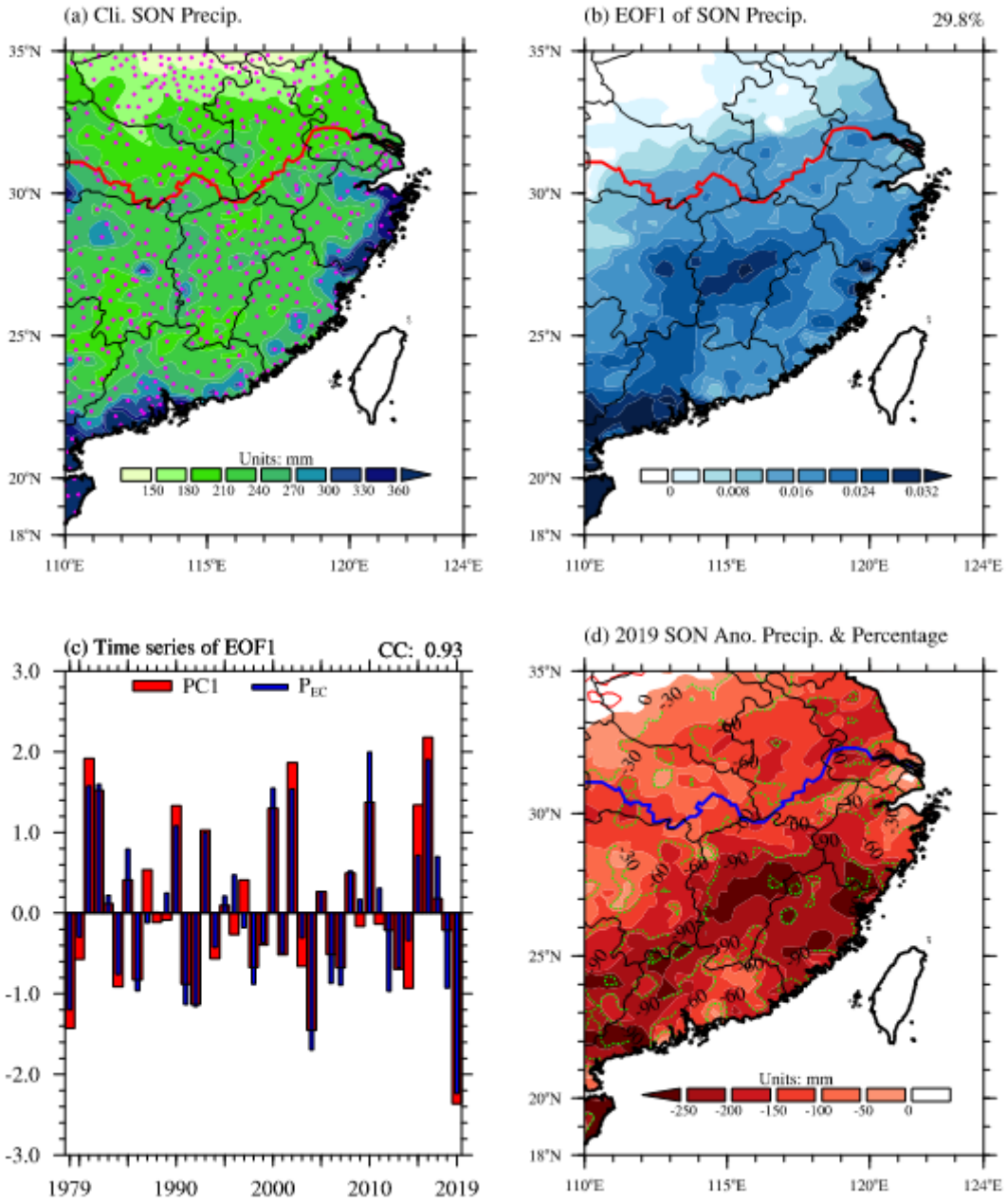

Figure 1

(a) Climatological mean autumn precipitation (units: mm) over the eastern China. (b) Spatial distribution of the first EOF mode. (c) Normalized time series of the first EOF mode (broad red bars) and mean precipitation anomaly over the eastern China (narrow blue bars). (d) Distribution of precipitation anomaly (shading, units: mm) and its percentage (green dashed lines, units: %) during autumn in 2019 over the eastern China. Magenta dots in (a) denote the 604 observing stations. Red and Blue thick lines represent the Yangtze River in (a-b) and (d), respectively. The value on the upper right corner of (c) indicates the correlation coefficient between the time coefficient of the first EOF mode and precipitation anomaly averaged over the eastern China.

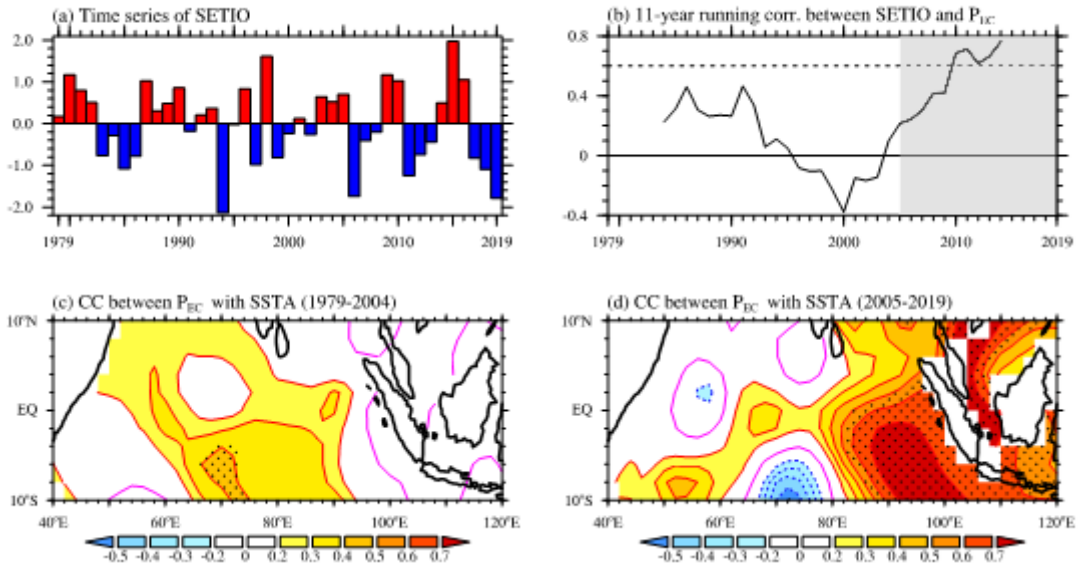

Figure 2

(a) The standardized time series of SSTA averaged over the SETIO region. (b) The 11-year sliding correlation coefficient between ISETIO and PEC. The dashed line indicates a statistical significance at the 95% confidence level estimated by the two-tailed t-test. Grey shading represents the period when ISETIO and PEC are closely correlated. The correlation coefficient between PEC and tropical Indian SST during (c) 1979-2004 (d) and 2005-2019. Stippled areas are of significant at the 95% confidence level, from a two-tailed t-test.

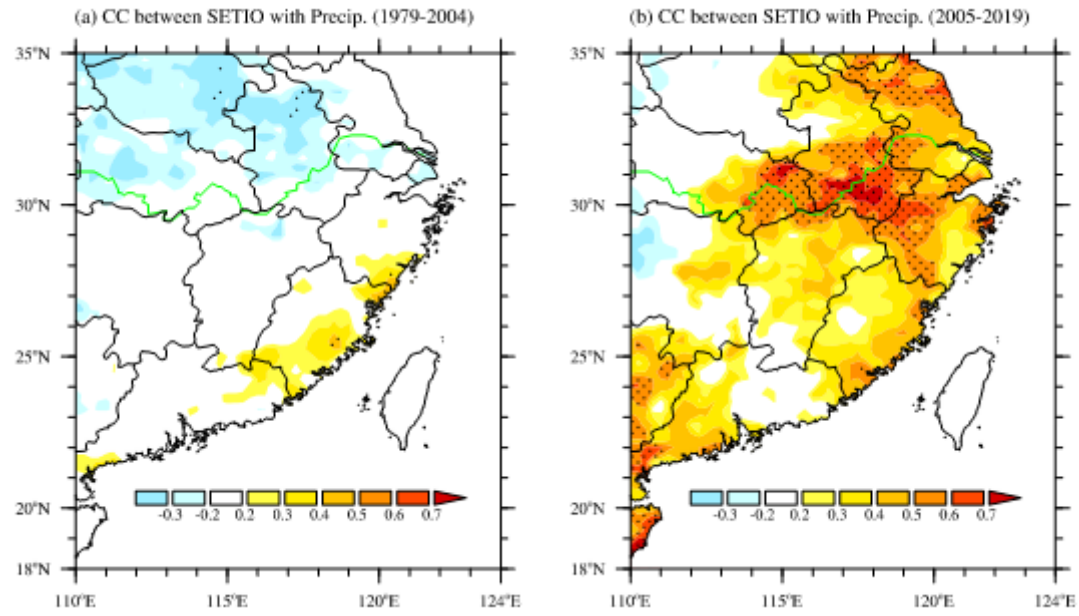

Figure 3

As in Figure 2 (c) and (d), but for the correlation coefficient between ISETIO and precipitation anomaly during autumn in 2019 over the eastern China.

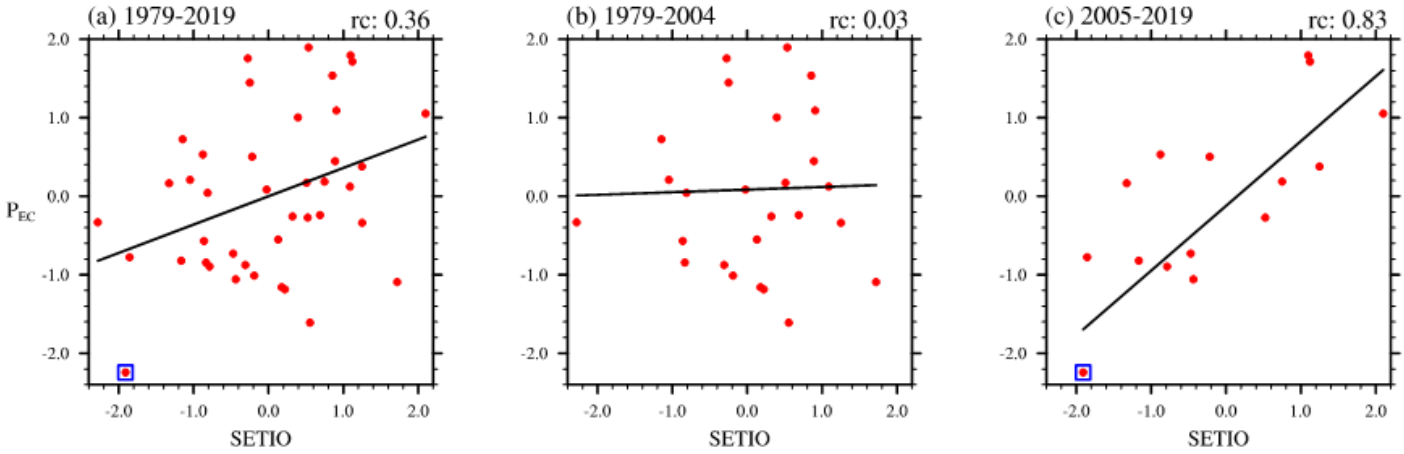

Figure 4

Scatter plot of ISETIO and PEC during (a) 1979-2019, (b) 1979-2004, (c) 2005-2019. Straight lines indicates the linear fitted lines. Linear fitted index (rc) is provided in the upper right corner of each panel. The red dots surrounded by the blue square in (a) and (c) represent the values of ISETIO and PEC in 2019.

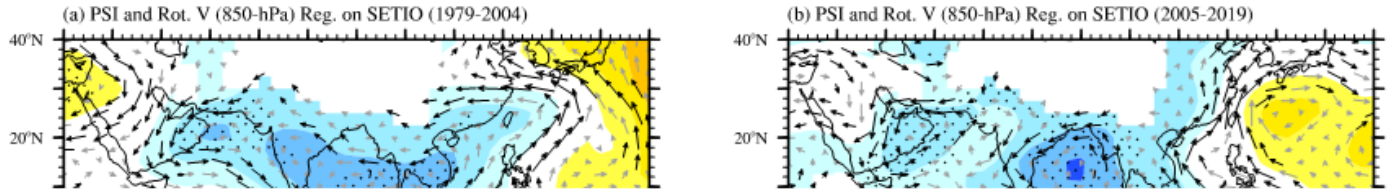

Figure 5

Regressed stream function (shaded, units: 105m2s-1) and rotating wind (vectors, units: ms-1) on 850 hPa during (a) 1979-2004, (b) 2004-2005. All fields are obtained by regressing these quantities onto ISETIO. Stippled areas and black arrows are for those exceeding the 95% confidence level.

Figure 6

As in Figure 5, but for regressed water vapour flux integrated from the surface to 300 hPa (arrows, units: kg·m−1·s−1) and its divergence (shading, units: 10−6 kg·m−2·s−1).

Figure 7

Regressed velocity potential (shading, units: 105 m2·s−1) and divergent wind (vectors, units: m·s−1) on (a) 850 hPa, and (b) 200 hPa. (c) Regressed vertical velocity (shading, units: Pascal·s−1) on 500 hPa. All fields are obtained by regressing these quantities onto ISETIO during 1979-2004. (c), (d) and (f) are as (a), (b), (c), respectively, but during 2005-2019. Stippled areas and black arrows are for those exceeding the 95% confidence level.

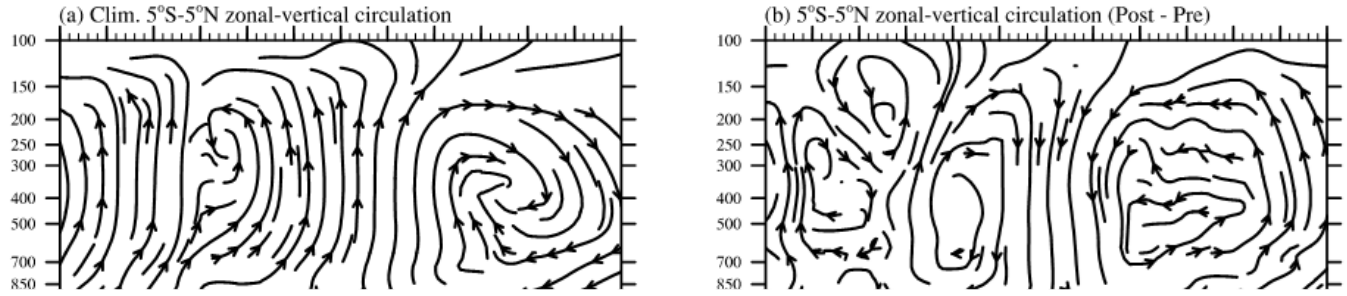

Figure 8

(a) Climatological mean equatorial (averaged over 5°S to 5°N) zonal-vertical circulation. (b) Differences of the regressed equatorial (averaged over 5°S to 5°N) zonal–vertical circulation with respect to the ISETIO for 2015-2019 and 1979-2004. Its horizontal component is the zonal component of divergent wind, and vertical component is the vertical velocity. (c), (d) as in (a), (b), respectively, but for the meridional–vertical circulation averaged over 110°E–122.5°E. Its horizontal component is the meridional component of divergent wind.

Figure 9

Anomalies of (a) SST over tropical Indian Ocean (units: ℃) in the autumn of 2019, and those of (b) streamfunction (shading, nuits: 105m2s-1) along with rotating wind (vectors, units: ms-1) on 850 hPa, (c) 850 hPa, and (d) 200 hPa velocity potential (shading, units: 105 m2·s−1) and divergent wind (vectors, units: m·s−1), (e) vertical velocity (shading, units: Pascal·s−1) on 500 hPa. The green lines denote the coastline in each panel, and (f) water vapour flux integrated from the surface to 300 hPa (arrows, units: kg·m−1·s−1) and its divergence (shading, units: 10−6 kg·m−2·s−1).